Proton-Collecting Properties of Bovine Heart Cytochrome *c* Oxidase: Kinetic and Electrostatic Analysis†

Yael Marantz,‡ Ólöf Einarsdóttir,§ Esther Nachliel,‡ and Menachem Gutman*,‡

Laser Laboratory for Fast Reactions in Biology, Department of Biology, The George S. Wise Facility of Life Sciences, Tel Aviv University, Ramat Aviv, Tel Aviv 69978, Israel, and Department of Chemistry and Biochemistry, University of California, Santa Cruz, California 95064

Received March 6, 2001; Revised Manuscript Received September 21, 2001

ABSTRACT: Proton-transfer reactions on the surface of bovine heart cytochrome *c* oxidase were investigated by combining a laser-induced proton-pulse technique with molecular modeling. The experimental approach simultaneously monitors the state of pyranine protonation in the bulk phase and that of a fluorescein indicator specifically attached to the native Cys(III-115) residue of subunit III of cytochrome oxidase. The reversible dynamics of the acid−base equilibration between the surface and the bulk phase were measured with submicrosecond time resolution and analyzed by numerical integration of coupled nonlinear differential rate equations. Kinetic analysis shows that carboxylates on the surface of the protein act as a proton-collecting antenna, which is able to rapidly transfer protons to nearby histidines that function as a local proton reservoir. These properties enable cytochrome oxidase to carry out its redox-linked proton translocation. Molecular modeling of the fluorescein-binding site indicates that, in addition to the covalent bond, the dye is anchored through a hydrogen bond to the hydroxyl moiety of Tyr(VII-50). The protonation of the dye is mediated through three residues that shuttle protons between the bulk and the dye. A correlation between the measured kinetic properties of the bound fluorescein and the different configurations of the dye allows us to predict the identity of the proton-binding sites in the fluorescein-binding domain.

Cytochrome oxidase catalyzes the reduction of dioxygen to water by electrons donated by cytochrome *c*. Four protons (scalar) are required for the redox reaction, and four additional protons are translocated across the membrane to generate an electrochemical proton gradient (*1*). While we have considerable knowledge about the electron-transfer steps in the redox reaction, the precise mechanism of proton transfer and its coupling to the redox reaction has not yet been established (*2*−*8*). On the basis of the recent crystal structures of the bovine and *Paracoccus* cytochrome oxidase, two major proton-transfer pathways have been proposed, the D-pathway and the K-pathway (*9*−*12*). The D-pathway transports both scalar and translocated protons during the reaction of O_2 with the fully reduced enzyme (*2*, *13*−*19*), while the K-pathway transports only scalar protons during the reduction of the oxidized enzyme (*2*, *13*, *15*, *16*, *18*, *20*, *21*).

Proton-linked energy-transducing enzymes, like the heme−copper oxidases, operate under restrictive conditions; protons must be taken up through a specific entry point from an environment where their concentration is 10^{-7} M or less, and the reaction must be completed within the temporal limits set by the turnover rate of the enzyme. At pH ≥7 and in the presence of 100 mM electrolyte, the time constant for proton binding should be longer than 1 ms. However, the experimentally measured time for proton uptake by cytochrome oxidase is significantly shorter (∼360 μs) (*22*), and individual steps can be much faster. This apparent paradox implies that protonation of the active site is not only by free protons but may be mediated by soluble and surface buffer groups which function as a local proton reservoir. At concentrations higher than few millimolar, mobile buffer molecules can also remove a proton from a site on a time scale much shorter than the turnover rate. Consequently, proton-translocating energy-transducing enzymes must have a mechanism suitable both for fast binding of protons and for retaining them secured from mobile buffer molecules. In the present study, we investigated this capability by generating an artificial proton-binding site on bovine cytochrome *c* oxidase.

During catalysis, cytochrome oxidase must accept protons from the well-buffered solution of the cytoplasmic space at rates faster than the catalytic cycle, while the dwell time of protons on the surface must be compatible with the turnover rate. Basic chemical considerations imply cooperative interactions between two types of residues: one that reacts rapidly with free protons and a second that retains them for longer periods and acts as a local reservoir. Recent proton-pulse experiments on *Rhodobacter sphaeroides* cytochrome *c* oxidase have shown that both functions are mediated by a "proton-binding antenna" and high connectivity in the form of fast shuttling of protons between carboxylate and histidine residues on the surface of the enzyme (*23*).

† This work was supported by American Israeli Bi-National Science Foundation Grant 97-00130 (M.G.) and National Institutes of Health Grant GM 53788 (Ó.E.).

* To whom correspondence should be addressed. E-mail: me@hemi.tau.ac.il. Fax: 972-3-6406834.

‡ Tel Aviv University.

§ University of California, Santa Cruz.

10.1021/bi010453w CCC: $20.00
Published on Web 11/17/2001

In this paper, we have investigated the dynamic proton processes taking place on the surface of bovine heart cytochrome *c* oxidase. The simultaneous monitoring of the protonation state of pyranine in the bulk phase and a fluorescein (Flu)[1] indicator covalently attached to Cys(III-115) on the intermembrane face of subunit III of cytochrome oxidase permits calculation of the rate constants of protonation of all reacting groups, their p*K* values, and how fast they can exchange protons among themselves. Our kinetic analysis shows that the surface is composed of a proton-collecting antenna (carboxylates), which is able to rapidly transfer protons to histidine moieties on the surface. The binding of the Flu to different locations on the protein shows that the protonation dynamics of a specific location are controlled by the detailed topography of the various proton-binding sites located within 20 Å of the indicator. Using molecular modeling, possible orientations of the Flu molecule were calculated, and the most stable configuration was found to be arranged in a manner consistent with the measured rate constants.

MATERIALS AND METHODS

Labeling of Cytochrome Oxidase by Fluorescein. Bovine heart cytochrome *c* oxidase was prepared by the method of Yoshikawa et al. (*24*). The final pellet was dissolved in 10 mM sodium phosphate buffer, pH 7.4, and dialyzed against the same buffer for 24 h. The enzyme was stored at −80 °C until use.

Fluorescein-5-maleimide (Flu) was added to a 30 μM enzyme solution in 10 mM phosphate buffer, pH 7.1, and 0.1% *n*-dodecyl β-D-maltoside (LM) in a molar ratio of 1:1. The mixture was incubated for 20 min at 25 °C, and the buffer and unbound Flu were removed on a Sephadex G-25 column equilibrated with 0.1% LM and 50 mM KCl, pH 7.5. The concentration of the enzyme was determined at 605 nm using an extinction coefficient of 24 mM^{-1} cm^{-1} for the reduced-minus-oxidized enzyme. The concentration of the Flu was determined at pH ∼8.5 from its absorbance at 500 nm, using an extinction coefficient of 63 mM^{-1} cm^{-1} (*25*). The labeled subunit was identified by SDS−acrylamide gel electrophoresis and was found to be Cys115 on subunit III.

To label other cysteine residues on the protein, cytochrome oxidase was incubated for 20 min with *N*-ethylmaleimide in a 1:1.2 ratio. Subsequently, fluorescein-5-maleimide was added in a 1:1 ratio and the solution incubated for an additional 2 h. This incubation resulted in labeling (85%) on several subunits, I, V, and VIII, as shown by SDS gel electrophoresis. Subunit III was not labeled by the fluorescein dye as it was blocked by the *N*-ethylmaleimide.

Enzymatic Activity. Cytochrome oxidase activity was measured spectrophotometrically at pH 6.0 following the oxidation of reduced horse heart cytochrome *c* at 550 nm (*26*). The horse heart cytochrome *c* (Sigma) was first reduced by ascorbic acid, and the excess reductant was removed by a PD-10 column.

Proton-Pulse Experiments of Bovine Cytochrome c Oxidase. Cytochrome *c* oxidase (final concentration 1−6 μM) was added to 1 mL of 50 mM KCl containing either 14, 21, or 27 μM pyranine. The sample was placed in a 1 × 1 cm cuvette and continuously stirred by a magnetic bar. The pH of the solution was monitored by a glass electrode and adjusted by the addition of small amounts of HCl or NaOH. The reaction mixture was excited by a short laser pulse (Nd:YAG laser, $\lambda = 355$ nm, 2 ns fwhm, 1.6 mJ/pulse, 10 Hz), which caused a transient dissociation of pyranine into a proton and a pyranine anion, thereby producing a very rapid proton pulse. The concentration of the resulting pyranine anion was monitored by an Ar laser probe beam (458 nm) and converted to a molar concentration using a differential extinction coefficient (alkaline-minus-acidic) of pyranine, $\Delta\epsilon = 24000$ M^{-1} cm^{-1}. The protonation of fluorescein was measured at 496 nm using a differential extinction coefficient (alkaline-minus-acidic) of 50000 M^{-1} cm^{-1}.

Kinetic Analysis. The response of the reaction system to the pH change is a summation of many parallel, tightly coupled reversible reactions that fall into two categories. The first category is the diffusion-controlled reaction between the proton (or the pyranine anion) and the protein-bound proton-binding sites. The second mechanism is a proton exchange between the fixed proton-binding sites of the protein. This exchange proceeds in a local environment where the density of the reactants, separated from each other by 3−10 Å units, is comparable to that of a homogeneous solution having a concentration of 1−4 M.

The relaxation dynamics between the surface and the bulk phase can be reconstructed by a set of coupled nonlinear, first-order, differential rate equations that comply with the detailed balance principle (*27*−*33*). The equations account for all proton-transfer reactions between each component $\{R_i\}$ and each of the other proton-binding sites $\{R_j\}$ present in the system:

$$dR_i/dt = k_{diss}\{RH_i\} - k_{as}\{R_i\}\{H^+\} + \sum k_{ji}\{RH_i\}\{R_j\} - \sum k_{ji}\{R_i\}\{RH_j\} \quad (1)$$

The term k_{diss} corresponds to the dissociation rate constant of the acid RH_i, k_{as} is the rate constant of the reaction of R_i with free protons, $\sum k_{ji}\{RH_i\}\{R_j\}$ is the sum of all reactions in which $\{RH_i\}$ functions as a proton donor to other proton-binding sites, and $\sum k_{ji}\{R_i\}\{RH_j\}$ is the sum of the back-reactions where $\{R_i\}$ is the acceptor with respect to all other proton-binding sites. The same equations, with the appropriate rate constants, are given for each reactant in the system and are linked in a manner complying with the mass conservation law. The mathematical model is comprehensive and accounts for every proton-transfer process in the solution with no approximation.

Our analytical approach has the same rationale as the deduction of a structural model from an X-ray diffraction pattern, where a number of independent observations are reconstructed by a single set of diffracting elements placed at defined coordinates. In the results described here, all of the independently recorded kinetic tracings were simulated by a single set of rate constants. With the correct selection of rate constants, the integration is a reconstruction of the observed dynamics. To increase the accuracy of the reconstruction, the signals were analyzed in pairs, reconstructing simultaneously both the pyranine and fluorescein signals that

[1] Abbreviations: ΦOH, pyranine (8-hydroxypyrene-1,3,6-trisulfonate); ΦO^-, pyranine anion; Flu, fluorescein; Flu^-, deprotonated fluorescein; LM, *n*-dodecyl β-D-maltoside; Cys(III-115), cysteine 115 of subunit III.

were measured at the same pH value (*23*, *34*). An acceptable reconstruction is one in which the kinetic traces of both dyes are matched by the calculated curves to the same degree of accuracy.

The reconstruction of a single pair of kinetic traces has a considerable range in terms of selected rate constants. Yet, as the number of independent, nonidentical signals increases, the solutions converge to a single set of rate constants that describe all of the experimental results. Recent application of a genetic algorithm procedure for proton-pulse measurements, with 12 independent adjustable parameters, indicated that the system converges to a single global minimum (Fibich and Nachliel, unpublished results).

In principle, each proton-binding site of the protein should be individually expressed, but this is analytically too demanding. In the approach described here, the system was simplified by grouping the reactive residues into subpopulations, each characterized by common equilibrium and rate constants. The reconstruction of the pyranine and the fluorescein signals is a summation of all parallel reactions that link the transient protonation of moieties in the bulk, on the protein's surface, the two dye molecules, and the residues located in the immediate vicinity of the bound fluorescein. This analytical approach and results will be described in the text while the rate constants are summarized in Tables 1 and 2.

Calculation of the Surface Potential of Cytochrome c Oxidase. Electrostatic potential maps of the surface of cytochrome oxidase were generated using the software package GRASP. The atomic coordinates were based on the PDB entry 1occ, after hydrogen atoms were added (*35*). The partial charges and size of the atoms were taken as parametrized and listed in the PARSE program (*36*). Since the GRASP program cannot handle a protein as large as cytochrome *c* oxidase, the PDB file was divided into two separate files that contained either the subunits facing the intermembrane space or the matrix side of the enzyme. An in-house computer program was used to analyze the PDB files and calculate distances between proton-binding residues and to identify which of the anionic residues on the surface of the protein were masked by a nearby positive charge.

Structural Analysis of Cytochrome c Oxidase Using the Insight II Program. The energy calculations were carried out using the Discover module of the Insight II program package. All minimizations utilized the consistent valence force field (CVFF) without any cross-terms. Structures were initially minimized using the steepest descent algorithm, followed by the conjugated gradient algorithm, with the gradient convergence criterion set to 0.001 kcal/(mol·Å). The calculations were conducted using dielectric constants of $\epsilon = 20$ and $\epsilon = 80$. To avoid excessive calculation time, the energy minimization was carried out on a limited portion of the enzyme, defined by a 20−30 Å radius from the sulfur atom of Cys(III-115).

The modeling of the bound fluorescein-5-maleimide to the sulfur atom of Cys(III-115) was carried out after structural relaxation of the protein. The fluorescein-5-maleimide−cysteine adduct can exist in four stereo conformers (3*R*, 3*S*, 4*R*, and 4*S*, referring to the carbon−sulfur bond geometry), which may differ in their free energy. The various adducts were generated with different initial orientations of the dye with respect to the protein. Each configuration was carried through a set of minimization procedures, and the final total free energy of the adduct was recorded.

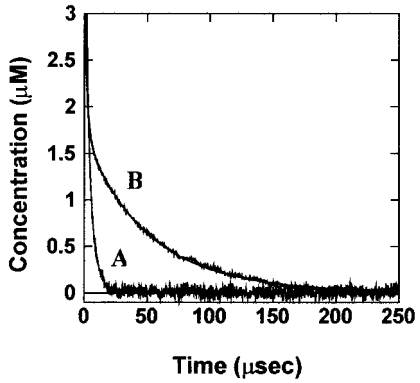

FIGURE 1: Reprotonation kinetics of pyranine following photoexcitation. The concentration of pyranine was 30 μM, and the kinetics were monitored in either the absence (curve A) or the presence (curve B) of 1 μM cytochrome oxidase, pH 7.1 (50 mM KCl, 0.1% LM). The *y*-axis represents the incremental concentration of the pyranine anion generated by the laser pulse and the relaxation corresponding to its reprotonation. The smooth lines are the simulated course of the reactions reconstructed by a numeric integration of a set of coupled nonlinear homogeneous differential rate equations with the rate constants as adjustable parameters.

RESULTS

Kinetic Analysis of the Acid−Base Perturbation. Figure 1 shows the transient photodissociation of a pyranine (ΦOH) solution (30 μM), either in an unbuffered salt solution (curve A; 50 mM KCl, 0.1% LM) or in the same solution but supplemented with 1 μM bovine cytochrome *c* oxidase (curve B). At zero time, a 2 ns laser pulse ($\lambda = 355$ nm, 1.6 mJ/pulse) excites the pyranine to its first electronic singlet state. Excitation of the pyranine shifts the p*K* of the pyranine from $pK_0 = 7.7$ down to $pK^* = 1.4$, causing a proton to dissociate from the excited molecule with a time constant $\tau = 120$ ps. After relaxation of the excited anion to the ground state ($\tau = 6$ ns), it regains its high p*K*, but the system is in a temporary state of acid−base disequilibrium. The discharged protons react in a diffusion-controlled reaction with all components present in the system (mobile buffers or the proton-binding groups on the protein). The reprotonation of the ground-state pyranine anion was measured by an incremental absorption at 458 nm. The slower relaxation of the signal in the presence of the enzyme reflects the delayed reaction of the protein-bound protons with the pyranine anion.

The continuous lines in Figure 1 superimposed on the experimental data (hardly observed due to the quality of the fit) show the in silico reconstruction of the reaction. The reconstruction of curve A was readily obtained by integration of differential rate equations compatible for a system consisting of pyranine in an aqueous solution (*27*). The reconstruction of the curves measured in the presence of cytochrome oxidase requires information regarding the number of proton-binding sites available for the reaction with the free proton within a time window of a few microseconds and their p*K* values and rate constants.

Proton-binding sites with p*K* values higher than 8.5 (like lysine and arginine residues) are unlikely to participate in the reversible protonation of the protein since they are initially almost entirely protonated. Similarly, residues with

p*K* ≤4 retain protons for a very short time ($\tau \leq 1$ μs), with little effect on reprotonation of the pyranine. Moreover, proton-binding sites that are not exposed to the bulk phase can also be excluded from the fast reversible reactions with free protons. It follows that the number of proton-binding sites responsible for the measured transients is smaller than the total number of carboxylate and histidine residues.

Attempts to reconstruct curve B in Figure 1, by assuming that all 147 carboxylates react with the free proton, failed to approach even the shape of the measured curve. A fair approximation required that the number of reacting carboxylates be reduced to 40−60. Similarly, if the total number of histidine residues were assumed to be reactants in the reconstruction, the resulting transients were too slow to fit the observed signals. The reconstruction of the signal was feasible only when the estimated number of histidine residues was in the range of 20−40.

The necessity to reduce the number of rapidly reacting proton-binding sites to less than the total number should be supported through a correlation between the number of residues determined by the kinetics and the structure of the protein. Out of the 147 carboxylates, 65 histidines, and 130 basic residues present in the bovine enzyme, 10 carboxylates and 15 histidine residues are embedded in the structure and will not react with the protons in the bulk phase within the submillisecond time frame of the pH-jump experiment. The rest of the residues should be considered in terms of their p*K* values. A single carboxylate on a surface of a low dielectric matrix has a p*K* ≥4. A residue with such a p*K* can retain a proton in the bound state for a few microseconds, a period long enough to decrease the reprotonation rate of pyranine (*37*). However, a positive charge in the immediate vicinity of the carboxylate can lower its p*K*, thus shortening the lifetime of the protonated state to less than 1 μs (*38*). Gunner and co-workers have carried out intensive calculations looking for the effect of nearby charges on the p*K* value of proton-binding sites in the *Rhodopseudomonas viridis* reaction center (*39*, *40*). It was found that even when the charges were partially buried ($\epsilon \leq 6$), a separation of ∼8 Å between the residues lowered the cross-interaction to less than 2 p*K* units. Thus we argue that, at the protein surface where the effective dielectric constant is at least 10 times larger, a positive charge located more than 8 Å from a carboxylate will have a small effect on its p*K* value and the dwell time of the proton will be long enough to be detected by the kinetic measurements. On the other hand, carboxylates that have a neighboring positive charge(s) at less than 8 Å will be too acidic to affect the reprotonation dynamics of the pyranine anion.

An in-house program called pair analysis was used to estimate the number of carboxylates with p*K*s that might be lowered by nearby positive residues. Using this procedure, 105 out of 147 carboxylates were found to be within 8 Å (or less) from lysine or arginine residues. However, about 20 out of the 105 are also located in proximity to other negatively charged residues. Consequently, the effect of the positive moieties might be reduced, and some of these carboxylates will react with protons within the time of the experiment. Accordingly, the number of unscreened carboxylates that are exposed on the surface can be estimated to be ∼40. The p*K* of a histidine residue is close to 7. However, at a distance less than 8 Å from a negative charge, its p*K* will be higher. The residue therefore will be mostly in the protonated state and will not function as a proton-binding site. The pair analysis program identified 25 histidine residues that are less than 8 Å from carboxylate residues. Summing the high p*K* histidines and those excluded from the surface, we estimate that the number of histidine residues active in the transient bulk-surface proton transfer is ∼20. These findings are in accordance with the kinetic and thermodynamic parameters found in our kinetic analysis.

More detailed information regarding these parameters of the matrix side and the intermembrane-facing side of the oxidase can be gained by binding an indicator dye to only one side of the protein. The indicator can exchange protons only with the residues located on the side of the attachment, and the thermodynamic and kinetic parameters of each side can be deduced.

Binding of Fluorescein Maleimide (Flu) to Bovine Cytochrome c Oxidase. Cytochrome *c* oxidase contains 19 cysteine residues located on 10 different subunits. In the late 1980s Malatesta and Capaldi (*41*) showed that iodoacetamide, at a 1:1 molar ratio, reacts exclusively with cysteine 115 on subunit III. Incubation of the enzyme with eosin-5-maleimide also resulted in binding at the same site (*42*). In the present study, the incubation of bovine cytochrome *c* oxidase with fluorescein maleimide (at 1:1 molar ratio) for 20 min at 25 °C resulted in selective labeling (∼90%) of subunit III as verified by SDS gel electrophoresis. The labeled site is assumed to be Cys(III-115). This is supported by the X-ray structure (*12*), which shows that the only other cysteine located on subunit III, Cys(III-218), is not exposed to the surface. The labeling of the protein by fluorescein did not affect the activity or the spectrum of the cytochrome oxidase (data not shown).

The binding of the fluorescein to the protein alters the environment of the dye, causing p*K* and spectral shifts. On binding to the Cys(III-115) residue of cytochrome oxidase, the spectrum of the fluorescein (in the alkaline state) was shifted from 496 to 501 nm (2090 cm^{-1}) and the p*K* increased to 7.7 when measured at $I = 100$ mM. Free fluorescein was found to have a p*K* of 6.3 under the same conditions. As will be discussed below, these two observations can be explained by the formation of a hydrogen bond between the dye and the hydroxyl residue of Tyr(VII-50), which is also hydrogen bonded to the nitrogen atom of Lys(VIII-84). These features are specific to the fluorescein attached at Cys(III-115). Blocking Cys(III-115) by *N*-ethylmaleimide, followed by an intensive treatment with fluorescein-5-maleimide (1:1 dye/protein), resulted in multiple labeling on subunits I, V, and VIII (data not shown). The p*K* measured for this multilabeled preparation was significantly lower (p$K = 7.0$, $I = 100$ mM), and no red shift was observed in the absorption spectrum.

Pulse Protonation of the Fluorescein-Labeled Cytochrome c Oxidase. Figure 2 shows the protonation dynamics measured in the presence of 30 μM pyranine with 3 μM fluorescein-labeled cytochrome oxidase [Cys(III-115)], pH 7.4 (panel A), or multilabeled protein at pH 6.9 (panel B). The difference in the pH between the two experiments is due to the difference in the p*K*s of the labeled protein. The reprotonation dynamics of ΦO^- and Flu^- were followed at 458 and 501 nm, respectively. It should be pointed out that the Flu signals are magnified 20-fold. The dynamics of the

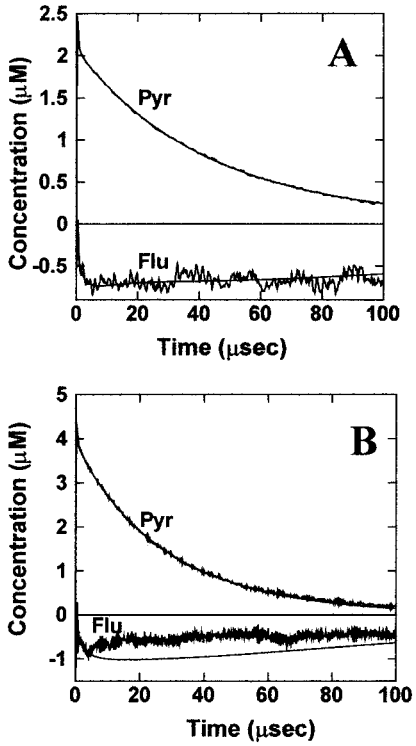

FIGURE 2: Proton-transfer dynamics between the bulk phase and the labeled bovine cytochrome *c* oxidase. Panel A: Cytochrome oxidase (3 μM) was labeled with fluorescein (Flu) (90% efficiency) on Cys(III-115), suspended in 30 μM pyranine (Pyr) (pH 7.4), and irradiated with a 355 nm laser pulse. The transient absorbance changes were measured at 458 and 501 nm for the ΦO^- and Flu, respectively. The fluorescein signals have been multiplied by 20 as reflected by the scale of the ordinate. The continuous lines represent the reconstruction of the observed dynamics, as generated by the numeric integration of the differential rate equations. Panel B: The transient absorbance changes were measured in the presence of 30 μM pyranine and 3 μM cytochrome oxidase labeled with fluorescein on other sites (subunits I, V, and VIII, 85% labeling) at pH 6.9. The simulation is based on the thermodynamic and kinetic parameters determined for the Cys(III-115)-bound fluorescein, and the difference between the data and the fit demonstrates the singularity of the solution.

fluorescein signal are characterized by a well-defined rise time, and the deprotonation phase is long, lasting more than 500 μs. Due to low-frequency electronic noise, a detailed analysis of the relaxation of the fluorescein signal could not be attained. Such a slow relaxation indicates that the dye is coupled by a proton-exchange reaction with a local proton reservoir, which maintains it in a protonated state.

The analysis of the kinetics measured with the Cys(III-115)−fluorescein-5-maleimide adducts of cytochrome *c* oxidase was carried out by reconstructing many independent pairs of kinetic tracings (ΦO^- and Flu^-), each measured under different initial conditions. The most convenient method to vary concentrations of the reactants is by changing the prepulse pH. In the present case, the high p*K* of the bound fluorescein limited the available pH range. At pH lower than 7, most of the fluorescein is initially protonated and its incremental absorption is negligible. At pH above 7.7, the ground-state dissociation of pyranine (pK = 7.7) lowers the concentration of the ΦOH state, reducing the number of released protons. Consequently, the measurements with the Cys(III-115)-labeled bovine oxidase were carried out in the narrow pH window of 7.2−7.4, and the large number of independent measurements, as required for accurate analysis, was attained by varying the concentrations of the reactants. The pyranine concentration was varied from 10 to 40 μM and the labeled protein from 1 to 4 μM. The measurements were carried out at two levels of time resolution, 2 and 10 ns per data point, corresponding to a total recording time of 25 and 100 μs, respectively. Altogether 21 experiments, in which both the pyranine and fluorescein were monitored, were subjected to kinetic analysis.

Kinetic Analysis. The analysis of the signal pair (pyranine and fluorescein) was initiated by modeling the relevant proton-binding sites of the protein. The reprotonation of the pyranine is affected by all exposed proton-binding sites and the rate of proton exchange between them, while the protonation of the fluorescein is mostly affected by the proton-binding capacity and the proton-transfer reactions in the immediate vicinity of the dye. Since Cys(III-115) is located on the intermembrane-facing side of the enzyme, its protonation dynamics are affected only by residues located on that face of the enzyme. Hence, the intermembrane- and the matrix-facing sides of the protein can be treated as two populations. Both affect the pyranine relaxation, but only one is linked to the fluorescein signal. The two populations exchange protons only through the bulk phase.

The strategy of the reconstruction was a stepwise increment of the complexity of the model. At first, the reconstructions were carried out with a minimal number of subpopulations. If the system failed, another subpopulation was introduced into the analysis. The procedure was terminated with the lowest number of subpopulations where a good fit of the signals was achieved. Table 1 lists the minimal number of populations of proton-binding sites that can reconstruct the pyranine relaxation curves. Increasing the number of subpopulations beyond that limit did not increase the quality of the reconstructed fit to the measured curves.

The proton-binding sites of the protein were divided into two classes, one for the matrix surface (in) and the other for the intermembrane-facing side of the oxidase (out). In each class, the proton-binding sites are referred to as low p*K* moieties (COO^-_{in} and COO^-_{out}). Similarly, the high p*K* residues will be referred to as His_{in} and His_{out}. Each of the four subpopulations was assigned an average p*K* and rate constants. While these populations were sufficient to simulate the pyranine dynamics, the complex dynamics of the Flu required the introduction of additional proton-binding sites located near the fluorescein. The minimal number of different proton-binding sites adjacent to the bound dye, in the present case, is three. The rate constants of the three sites with the free diffusing proton or pyranine anion and the rate of proton exchange among them are given in Table 2. The properties of these groups, termed A, B, and C, will be discussed below.

The numerical analysis according to this model was performed on 21 pairs of independent signals (pyranine and fluorescein) that varied in their initial conditions. The continuous lines overlaying the experimental curves in Figure 2A demonstrate the accuracy of the simulation.

The sets of rate constants and p*K* values describing the buffer capacity of the oxidase surface and the immediate surroundings of the fluorescein dye (Tables 1 and 2) represent the minimal solution of the system that is capable of reconstructing the entire set of experimental signals. A more simplistic model was inadequate for reconstructing the

Table 1: Kinetic and Thermodynamic Parameters of the Surface Proton-Binding Sites of Bovine Heart Cytochrome *c* Oxidase[a]

	COO^-_{out} ($N = 19$)	His_{out} ($N = 5$)	COO^-_{in} ($N = 19$)	His_{in} ($N = 13$)
p*K*	5.5	6.6	5.0	7.0
reaction with H^+ (M^{-1} s^{-1})	$(2.0 \pm 0.3) \times 10^{10}$	$(5.0 \pm 0.5) \times 10^9$	$(2.0 \pm 0.5) \times 10^{10}$	1×10^9
reaction with ΦO^- (M^{-1} s^{-1})	1×10^7	$(1.3 \pm 0.3) \times 10^9$	1×10^7	$(5.5 \pm 0.5) \times 10^8$
virtual second-order rate constants				
$COO^-_{out} + His_{out}$	$(2 \pm 1) \times 10^{10}$			
$COO^-_{in} + His_{in}$	$(3 \pm 1) \times 10^{10}$			

[a] *N* refers to the number of reactive groups in each type of reactant. The italics indicate reactions between reactants bound to the surface, and the rate constants are of virtual second-order reactions.

Table 2: Kinetic and Thermodynamic Parameters of the Proton Transfer in the Vicinity of the Bound Fluorescein[a]

	Flu	group A	group B	group C
p*K*	7.4	6.0	6.0	7.5
reaction with H^+	$(1.0 \pm 0.4) \times 10^{10}$	$(0.9 \pm 0.1) \times 10^{10}$	$(0.10 \pm 0.04) \times 10^{10}$	$(5 \pm 1) \times 10^8$
reaction with ΦO^- (M^{-1} s^{-1})	$<10^7$	$(5 \pm 1) \times 10^8$	1×10^8	1×10^7
protonation by COO^-_{out}	$<10^8$	$<10^7$	$(1.0 \pm 0.5) \times 10^{10}$	$<10^7$
proton exchange with His_{out}	$<10^7$	$<10^7$	$(1.0 \pm 0.5) \times 10^{10}$	$<10^8$
proton transfer to Flu		$(30 \pm 5) \times 10^{10}$	$(1.0 \pm 0.4) \times 10^{10}$	$(1.2 \pm 0.5) \times 10^{10}$
proton transfer from AH			$(0.6 \pm 1) \times 10^{10}$	$<10^7$
proton transfer from BH				$<10^7$

[a] The italics denote reactions between reactants bound to the surface, and the rate constants are of virtual second-order reactions.

signals while increasing the complexity did not improve the accuracy of the reconstruction.

Applying the parameters appropriate for the simulation of the fluorescein bound to Cys(III-115) to the signals measured with the fluorescein attached at multiple sites on the protein failed to reconstruct the proton dynamics of the Flu (Figure 2B). The deprotonation dynamics of the Flu dye measured for this multilabeled protein are markedly faster than the simulated data, which represent the protonation dynamics of Flu attached to Cys(III-115). Thus the sets of rate constants in Tables 1 and 2 describe the proton-binding properties of a particular domain of the protein and are not applicable to the dynamics of other domains.

DISCUSSION

On the basis of the kinetic analysis that simulates the observed signals, the entire set of proton-transfer reactions between the bulk phase and the surface can be reconstructed, including the transient protonation of the various subpopulations, which cannot be directly observed. Figure 3 shows the protonation dynamics of COO^-_{in}, COO^-_{out}, His_{in}, and His_{out}, together with the dynamics of the free proton (H^+). The curves were generated by integration of the differential rate equations using the parameters listed in Table 1. The free proton concentration (panel B, inset) increased instantaneously to its maximum level and relaxed to the prepulse level within 1−2 μs. The rapid disappearance of the free protons is consistent with a diffusion-controlled reaction involving the pyranine (not shown) and the various proton-binding sites. The fastest protonation appears to be that of the carboxylates, which reach a maximal level of protonation within less than a microsecond. The deprotonation of the carboxylates follows a complex pattern; the initial deprotonation rate is high and coincides with the protonation of the histidine residues (panel A, inset). After ~5−10 μs, the deprotonation rate decreases, and both the carboxylate and histidine residues are deprotonated in tandem, indicating a state of quasi-equilibrium.

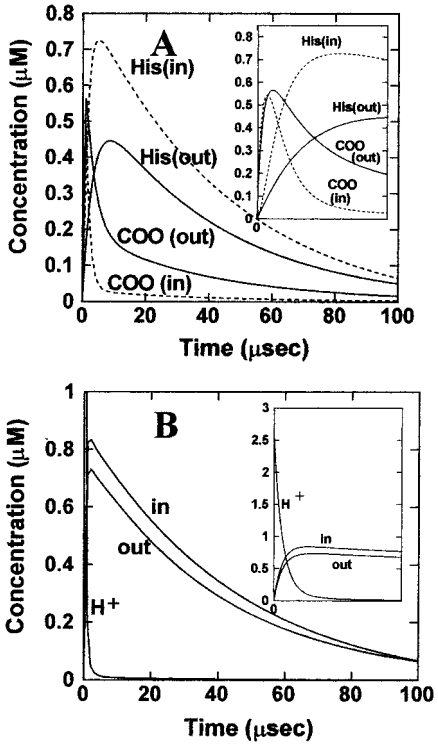

FIGURE 3: Detailed protonation dynamics between the bulk phase and the surface of cytochrome oxidase. The curves correspond to the experimental data presented in Figure 2. Panel A: Dynamics of the average carboxylate and histidine residues on the matrix side of the oxidase (in) and on the intermembrane-facing side of the protein (out). Inset: Initial (1−10 μs) events of the protonation of the average carboxylate and histidine populations. Panel B: Comparison of the temporal protonation profiles of all of the proton-binding sites on the intermembrane-facing side (out) and the matrix side of the enzyme (in).

The two faces of cytochrome oxidase differ in their reactivity toward protons as demonstrated by the simulation. Figure 3B summarizes the protonation state of all the proton-binding sites on each face of the enzyme. It is clear that the matrix face (in) is better adapted for binding protons.

Moreover, it should be pointed out that the calculation was carried out on the enzyme in a nonphysiological state, that is, without cytochrome *c* bound to its intermembrane-facing side. The binding of cytochrome *c* will block some of the negative sites, further reducing the proton-binding capacity of that surface (*43*). These results are consistent with the physiological role of the enzyme, which picks up protons from the well-buffered neutral pH matrix space and delivers them to the intraprotein-pumping element at the binuclear center of the enzyme.

Quantitative Evaluation of the Rate Constants. The kinetic and thermodynamic parameters listed in Table 1 represent intrinsic properties of the surface groups and, thus, merit quantitative interpretation. The carboxylates on the enzyme's surface react with free protons at a rate constant $k = 2 \times 10^{10}$ M^{-1} s^{-1}, a value at the upper range of a diffusion-controlled reaction of a single charged site on the surface of a protein (or a membrane) (*32*, *44*). In accordance with our previous experience, such a rate implies that the carboxylates are exposed and may even form clusters. The merged Coulomb cages of such clusters would accelerate their rate of protonation by forming a proton-collecting antenna with enhanced capacity to bind protons (*32*, *37*, *44*). It is of interest to point out that the rate constant for the protonation of the carboxylates measured for *R. sphaeroides* cytochrome oxidase (*23*) is of the same magnitude, or even faster (3×10^{10} M^{-1} s^{-1}). The histidine residues on the enzyme surface react with free protons at a slower rate (*23*). This rate constant is somewhat smaller than for a diffusion-controlled reaction, which indicates that the histidine residues are not fully exposed to the bulk phase.

The relationship between the state of protonation of the carboxylates and the histidines (Figure 3) implies that the two types of residues can exchange protons with high efficiency. This property is represented by the "virtual second-order rate constant", a term that denotes the rate of proton transfer between two sites fixed on the surface of a protein. As the sites cannot diffuse with respect to each other, the rate of proton transfer is not second order and the unit M^{-1} s^{-1} is not applicable. The introduction of virtual second-order rate constants enables us to correlate the measured rates with the distance and connectivity between the fixed proton-binding sites. Virtual second-order reactions with rate constants exceeding 10^{11} (virtual second-order rate constants are printed in italics) correspond to sites that are separated by one or two solvation shells (less than 10 Å apart). When the virtual second-order rate constant is less than 10^9, the sites are not connected by an effective proton-transfer system and proton exchange proceeds by diffusion through the bulk phase. Thus, the virtual second-order reaction between the surface carboxylates and histidine residues [$k = (2-3) \times 10^{10}$] represents good connectivity between the proton-binding sites in terms of fast proton transfer from the carboxylates to the histidines.

The deprotonation of the cytochrome oxidase surface has an apparent time constant $\tau \sim 75$ μs. This is too fast for spontaneous proton dissociation from the surface histidines, which according to their p*K* should retain the proton for almost 0.5−1 ms. Accordingly, the deprotonation of the surface of the protein proceeds by a collisional reaction between the free diffusing pyranine anion, ΦO^-, and the protonated residues on the surface. The calculated rate constant, $k = 1.3 \times 10^9$ M^{-1} s^{-1} (Table 1), is comparable in magnitude to a diffusion-controlled reaction (*32*). Assuming that a similar rate constant will apply to the reaction of the enzyme with other soluble buffer molecules, it is clear that the main pathway for equilibration between the enzyme and the surrounding bulk is not through dissociation but rather via collisional proton-transfer reactions with the buffer molecules. While this statement is valid for the overall protonation state, local deviations can be encountered, dominated by the immediate vicinity of the site, as we have observed for the bound fluorescein.

Evaluation of the Rate Constant of Proton Transfer in the Vicinity of the Fluorescein. The mechanism of proton transfer at the surface of the enzyme can be deduced by analyzing the protonation dynamics of the bound fluorescein. The bound dye reacts with free protons at a rate constant of 1×10^{10} M^{-1} s^{-1}, a typical value for a reaction between a free proton and a negatively charged group on the surface of a protein (Table 2). However, this reaction alone is not sufficient for reconstructing the complex protonation dynamics of the fluorescein. The accurate reconstruction of the fluorescein signals was impossible without the introduction of nearby proton-binding sites that modulated its dynamics. Assuming one or two "assistant" proton-binding sites were insufficient to gain high accuracy of reconstruction, three provided a satisfactory fit. Fitting the experimental curve with four nearby proton-binding sites was possible only if one of the sites was kinetically uncoupled from the fluorescein state of protonation. Thus, we regard the solution with three proton-binding sites that modulate the fluorescein dynamics as the most suitable one.

Groups A and B have the same p*K* value (p$K = 6$) but react with free protons at different rates, 1×10^9 and 9×10^9 M^{-1} s^{-1}, respectively. The third group, C, is much more basic (p$K = 7.5$) and reacts rather slowly, both with protons ($k = 5 \times 10^8$ M^{-1} s^{-1}) and the pyranine anion ($k = 1 \times 10^7$ M^{-1} s^{-1}) (Table 2). This indicates that group C is a partially buried moiety, which functions mostly as a local proton reservoir.

The virtual second-order rate constants of proton transfer between the three residues and the fluorescein allow us to deduce the connectivity between these sites. Group A reacts rapidly with the fluorescein moiety ($k = 3 \times 10^{11}$), indicating a very close proximity to Flu and sharing of solvating water molecules. Groups B and C transfer their protons to the Flu^- at slower rates, 1×10^{10} and 1.2×10^{10}. Thus, both groups are located about 10 Å from the two oxygen atoms of the dye. On the other hand, the proton-exchange reaction between groups B and C is very slow, suggesting that they are located on different sides of the fluorescein molecule.

The connectivity between the immediate vicinity of the fluorescein and the rest of the protein surface can be deduced by evaluating the virtual second-order reactions between the average carboxylates and groups, A, B, and C. Groups A and C have very weak connectivity with the average groups on the surface ($k \leq 1 \times 10^8$), implying that proton transfer between the surface residues and groups A and C occurs by diffusion in the bulk phase. On the other hand, group B has good connectivity with the surface groups.

Incorporation of these rate constants into the differential rate equations allowed us to analyze in detail the protonation dynamics of the fluorescein and groups A, B, and C. The

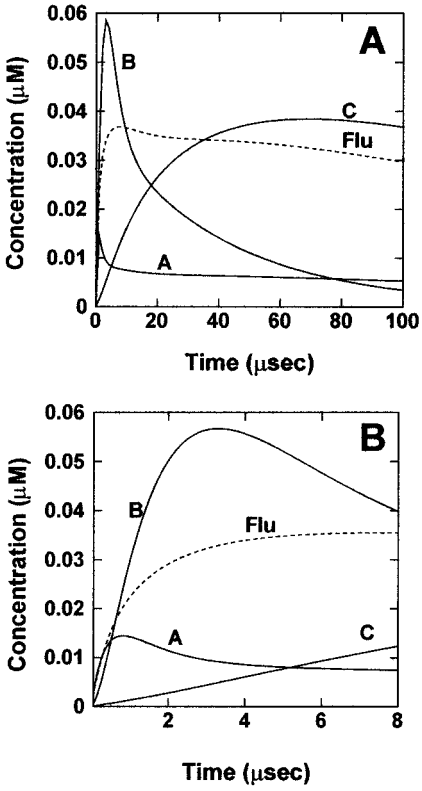

FIGURE 4: Detailed protonation dynamics of groups A, B, and C and fluorescein. The initial events (1−10 μs) are drawn in panel B.

results are presented in Figure 4. Panel A shows the dynamics over a 100 μs interval, with the initial 10 μs data shown in panel B. Groups A and B are the first to be protonated but not to the same extent. Group A, which reacts with free protons at a faster rate (Table 2), also transfers them to the fluorescein, and its protonation level declines to a steady-state within ~5 μs after the pulse. Group B is less accessible to free protons, yet is well connected to the "average" surface carboxylates. This, together with the slower reactions of group B with the fluorescein and group C, causes the maximal protonation state of group B to be higher than that of group A. The protonation of group C is mostly indirect, and its protons are obtained by equilibration with the fluorescein. Thus, group C acts as a local reservoir that slows the deprotonation of the fluorescein.

Electrostatic Potential of the Cytochrome c Oxidase Surface. The above kinetic analysis led to a series of structural predictions that can be confirmed by studying in detail the structure of the protein. To understand the differences between the proton-binding properties of the two faces of the oxidase, we used the GRASP program to map the electrostatic potential of each surface (Figure 5). The electrostatic potential maps of the two sides of cytochrome oxidase calculated at $I = 50$ mM are presented in Figure 5. Panel A represents the electrostatic potential of the intermembrane-facing side of the oxidase, while panel B shows the distribution of the acidic (red), basic (blue), and histidine (cyan) residues. The electrostatic potential and the amino acid distribution of the matrix surface are represented in panels C and D of Figure 5, respectively.

The electrostatic potential map of the intermembrane-facing side of the oxidase surface is mainly negative (colored

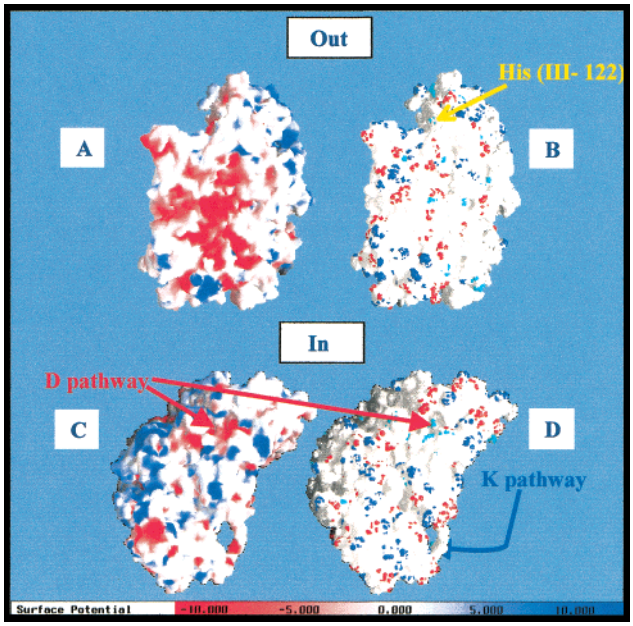

FIGURE 5: Electrostatic potential and distribution of the proton-binding groups on the surface of bovine heart cytochrome *c* oxidase. The electrostatic potentials of the intermembrane-facing side of the oxidase (out) (A) and the matrix side (in) (C) were generated by the GRASP program. Positions of the acidic, basic, and histidine groups on the intermembrane-facing side (B) and the matrix surface (D) are shown in red, blue, and cyan, respectively.

in red). The amino acid composition reveals that this negative potential is not a consequence of a large cluster of carboxylates but rather the absence of exposed basic groups next to them. The clustering of the carboxylates into continuous domains may account for the relatively high p*K* determined for the average population of carboxylates on the intermembrane face of the enzyme.

On the matrix surface (Figure 5C,D), the negative potential is concentrated in several patches, and a cluster of histidine residues is near the entrance of the D channel. During catalysis, cytochrome oxidase abstracts protons from the matrix space and releases them on the other side. At pH 7.4, the time constant of a free proton reacting with a site on the enzyme is ~1.2 ms [$\tau = 1/(k_{on} \times 10^{pH})$], which is slower than the rate of proton pumping by the enzyme (*22*). Apparently, an efficient proton-collecting antenna facilitates the protonation of the protein, and the charge distribution on the matrix face has the elements required for forming the antenna. The negative potential "patches" (the carboxylates) act as primary proton attracting sites, while the histidine residues that are located in close proximity to these negatively charged patches are the local reservoir that retains the protons on the surface for a long time.

Two proton-uptake pathways have been proposed as originating on the matrix surface: the D-pathway that funnels ~6 H^+/turnover, and the K pathway that transports only ~2 H^+/turnover (*2*, *13*−*21*). The entrance to the D-pathway is indicated in Figure 5C,D. The entrance to the K-pathway cannot be observed from this angle of presentation, but its location is indicated by an arrow. According to the calculated electrostatic potential map of the molecule, the entrance to these two pathways is negatively charged. The difference between the two is the amino acid composition of their immediate surroundings (Figure 5D). The only cluster of

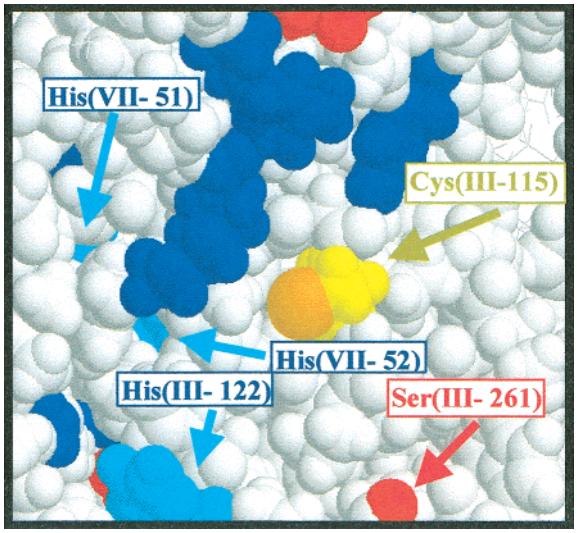

FIGURE 6: Detailed structure around Cys(III-115). A presentation of the domain of cytochrome oxidase within 20 Å from the Cys-(III-115) (drawn in yellow) is shown. The acidic [carboxylates + the C-terminal residue, Ser(III-261)], basic, and histidine groups are shown in red, blue, and cyan, respectively.

histidine residues on the protein is located at the entrance to the D-pathway (colored in cyan). Fewer and well-dispersed histidine residues are located at the entrance to the K-pathway. Thus, the negatively charged residues attract the protons and shuttle them to the cluster of histidines. Brzezinski and co-workers have attributed the difference in the numbers of the histidines to the slower rate of proton flux through the K-pathway (*20*).

Characterizations of the Proton-Binding Residues near the Bound Flu. Our proposed putative mechanism of proton transfer near the K- and D-channels is further supported by proton-transfer reactions near the bound fluorescein, where few histidine residues are present. Figure 6 is a detailed map of a domain centered around Cys(III-115), with the acidic, basic, and histidine residues within 20 Å from the cysteine shown in red, blue, and cyan, respectively. Three histidine residues, His(VII-52), His(III-122), and His(VII-51), were found at distances of 8.5, 11.5, and 14 Å, respectively, from the sulfur of Cys(III-115). Two carboxylates, Asp(III-190) and Asp(VIII-35), are located 14 Å from the sulfur atom. Both carboxylates are in close proximity (4 Å) to arginine residues, and therefore their p*K* is expected to be low. Another proton-binding group in the domain is the C-terminus of subunit III, Ser(III-261), located 10 Å from the sulfur atom. With so many possible proton-binding sites surrounding the fluorescein-binding sulfur atom, a more definitive procedure must be adopted before the reactive residues that determine the dynamics can be assigned to specific amino acid residues.

The C−S bond between the fluorescein-5-maleimide and the sulfur allows a free rotation of the dye. As a result, the precise placement of the chromophore with respect to the various residues in the domain is uncertain. However, the kinetic analysis indicated the presence of three residues with specific rate constants of proton transfer. Accordingly, we searched for a possible orientation of the fluorescein that would be consistent with the conclusions of the kinetic analysis.

Determination of the Orientation of Flu on the Cytochrome Oxidase Surface Using Energy Minimization Calculation. The calculations were carried out using the bovine cytochrome oxidase coordinates (PDB entry 1occ) following addition of hydrogen atoms and relaxation of the structure. To find the most stable conformation of the dye, the fluorescein-5-maleimide was covalently bound in its four possible conformers (3*R*, 3*S*, 4*R*, and 4*S*) to the sulfur atom of Cys(III-115). A search was carried out for each conformer, seeking the most stable orientation of the dye. At least five initial orientations were tested for each of the four conformers. The outcomes of the calculations were evaluated by relating the final orientation to the total free energy of the system ΔG_{total} (measured in kT units). These values should be considered only on a relative scale.

The most stable conformation has the structure shown in Figure 7A. A prominent feature of the structure is the hydrogen bond between the oxy atom of fluorescein and the hydroxyl residue of Tyr(VII-50). The nearby lysine, Lys-(VIII-84), is also at a hydrogen-bonded distance from the oxy atom of Tyr(VII-50). The interaction between the positive charge of the lysine, the π orbitals of the tyrosine, and the fluorescein chromophore are sufficient to stabilize the excited state of the dye, causing the red shift (2090 cm^{-1}, equivalent to a stabilization energy of 5.9 kcal/mol) of its absorption spectrum. The p*K* shift of the bound fluorescein ($\Delta pK \geq 1.4$, equivalent to $\Delta G \geq 2$ kcal/mol) is also compatible with the stabilization of the protonated state of the fluorescein by the hydrogen bond with the tyrosine.

The proton-binding sites deduced by correlating the kinetic analysis with the projected structure can be identified by comparing the observed rate constants with the distances between plausible proton-binding sites and the fluorescein acceptor. We assume that a shorter distance between a proton donor and an acceptor reflects a faster reaction rate. The proton donor nearest to the oxy atom of the fluorescein is the hydroxyl moiety of Tyr(VII-50). This residue forms a hydrogen bond with the dye and therefore should exchange a proton at a rate constant much faster than 3×10^{11} (*33*). Because we did not observe such a fast reaction, we suggest that the p*K* of the tyrosine is too high to protonate the indicator. Thus, the tyrosine is probably an anchoring point rather than a proton donor with respect to the dye. The nearby residues that can serve as proton donors are His(III-122), His(VII-52), and the terminal carboxylate of Ser(III-261), which are located 7.8, ~8.8, and ~13.8 Å, from the oxy atom of the dye, respectively.

The projected proximity of His(III-122) to the dye initiated a second set of calculations where the minimization was carried out with the histidine residues already protonated. The resulting most stable structure is shown in Figure 7B. In this configuration, the anchoring hydrogen bond with the tyrosine residue is as tight as before, but the dye has gained extra stability by a reduced distance (4.8 Å) between the oxy atom of the fluorescein to His(III-122). The tilting of the dye has also reduced the distance to Ser(III-261) to 11.7 Å, and Glu(III-128) is now located 12.7 Å from the dye.

Tentative Identification of the Proton-Binding Sites Next to the Fluorescein. The rate of protonation of the bound dye is a sum of its reaction with free protons and proton-exchange reactions with the three projected residues A, B, and C, whose properties are given in Table 2.

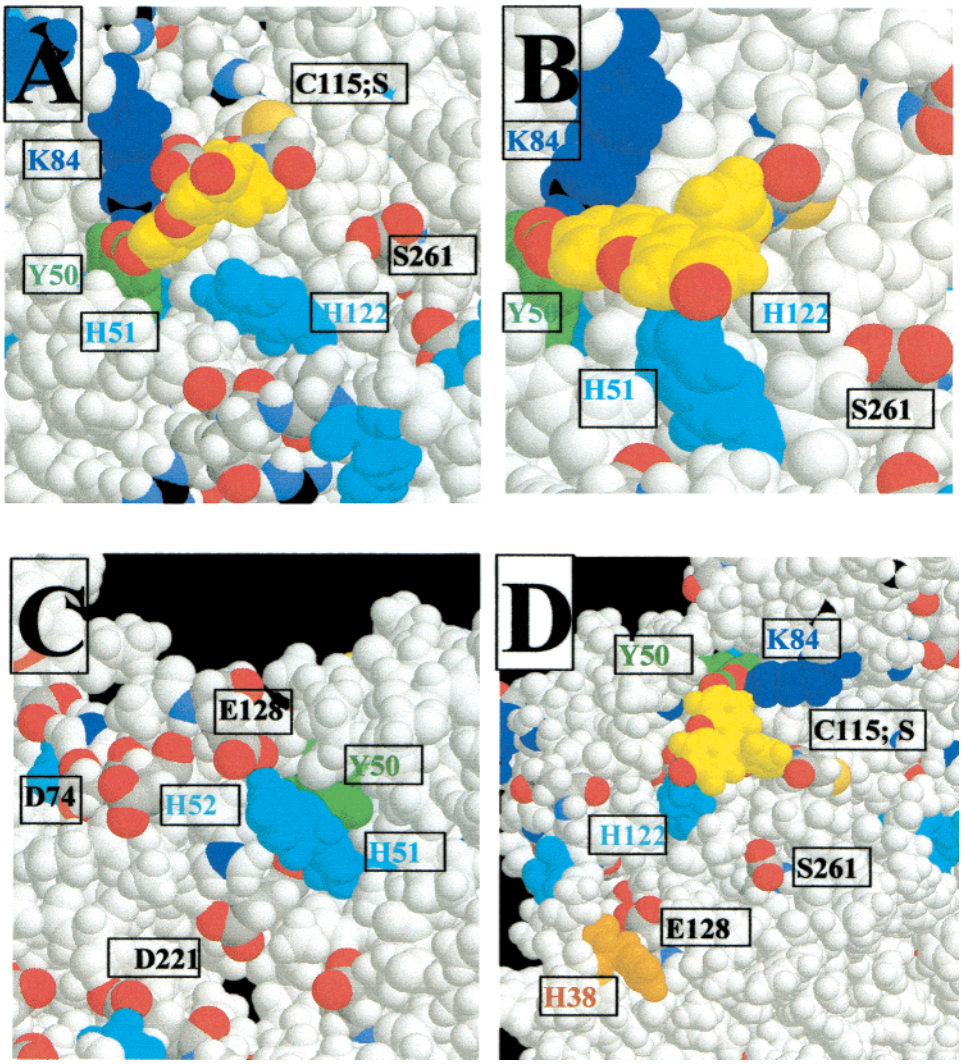

FIGURE 7: Minimum energy position of the Flu on the surface of bovine cytochrome *c* oxidase as determined by minimization calculations using the Discover program. Panel A corresponds to the most stable conformation in which His(III-122) is unprotonated. The separation between the oxy atom of the dye from the nearest nitrogen atom of the imidazole residue is 7.28 Å. Panel B corresponds to the most stable conformation that resulted from minimization calculations assuming His(III-122) was initially protonated. The interactions of the dye with Tyr(VII-50) and Lys(VIII-84) are as in panel A, but the dye's ring structure is tilted further toward the charged histidine, thereby reducing the distance between the oxy atom of the dye and the nearest nitrogen atom of the imidazole residue to 4.8 Å. As a result, the distance to the C-terminal moiety is shortened to 11.7 Å. Please note that the dye is connected through a narrow 8 Å long channel (larger than the diameter of a water molecule) with His(VII-51) (colored in cyan and seen in panels A and B). Panel C depicts the immediate vicinity of His(VII-51) and His(VII-52). The surrounding carboxylates located within a range of efficient proton transfer to the histidine residues are marked in the panel. Panel D depicts the two putative residues that can serve as group C, the C-terminal carboxylate, Ser(III-261), and Glu(III-128).

According to the kinetic analysis, group A is well exposed to the bulk. This conclusion is based on the diffusion-controlled rate constants for its reaction with free protons and with the pyranine anion. Group A is also in close proximity to the chromophore, as reflected by the rate of proton exchange between them ($k = 3 \times 10^{11}$). Examination of the structures presented in Figure 7A,B suggests that His-(III-122) is the most suitable candidate for group A. It is well exposed, and therefore, its p*K* value will be close to that of a histidine residue (p$K \sim 6$). Moreover, its distance to the proton-binding oxy atom of the dye is consistent with a virtual second-order rate constant of 10^{11}. Indeed, it is possible that the protonation of the histidine initiates a rapid local rearrangement of the structure, where the dye is slightly tilted toward the histidine. Therefore, the measured rate constant may not be that of the proton transfer (which for a separation of 4.8 Å can exceed 10^{11}) but instead represents the shifting of the chromophore.

Group B reacts with free protons at a rather slow rate, is hardly accessible to the pyranine anion, but is in a rapid equilibrium with the surface carboxylates. This functional residue is well connected with the chromophore, as indicated by a virtual second-order rate constant of $k = 10^{10}$. The rate of proton transfer between group B and the fluorescein suggests a separation of ~10 Å (*33*). Of all the residues located near the chromophore, His(VII-51) and His(VII-52) are the most appropriate for group B. His(VII-51) is ~9 Å from the oxy atom of the bound fluorescein (Figure 7A,B), connected with the dye through a channel running between Tyr(VII-50) and Gly(III-120). The channel is wide enough to allow penetration of a water molecule, thus making it suitable to function as a proton-conducting pathway. The two

histidine residues extend through a ridge of the protein and are surrounded by a cluster of carboxylates, including Glu(VIII-78), at a hydrogen-bonded distance from His(VII-51), Glu(III-111) at 9.9 Å, Asp(VII-74) at 7.8 Å, and Asp(I-221) at 10.3 Å. This ring of carboxylates can account for the fast proton transfer between the surface carboxylates and group B.

Group C has a rather high p*K* and a limited accessibility to free protons and the pyranine anion. According to the rate constant of proton exchange with the dye, it is located 10−15 Å away. Of all nearby residues which are ∼15 Å from the fluorescein, there are two possibilities for group C. These are the C-terminal carboxylate, Ser(III-261), at a distance of ∼11 Å from the oxy atom of the fluorescein and Glu(III-128), which is 12.6 Å away (Figure 7D). Both residues are located near the border between the charged fully exposed surface of the protein and the membrane-embedded section. It is possible that, in the detergent-solubilized form of the enzyme, Ser(III-261) and Glu(III-128) are within the detergent-covered domain, which limits their accessibility and results in a higher p*K* value.

CONCLUSIONS

In the present study, we have investigated to what extent kinetic measurements of proton transfer between the bulk phase and the surface of a large protein can yield structural information. The protein was labeled on a fortuitous SH residue, Cys(III-115), and its protonation dynamics were measured and analyzed. The results of this analysis allowed us to deduce the general features of the proton-binding capacity of the protein and provided a detailed analysis of the proton-transfer mechanism in the close vicinity of the bound pH indicator.

Cytochrome oxidase abstracts protons from the well-buffered neutral pH medium of the mitochondrial matrix and has an effective system for interacting with the bulk phase. This system consists of carboxylates, which serve as primary proton-binding sites, and histidine residues that function as a local proton reservoir. In agreement with the polarity of the enzyme, this function is more developed on the matrix-facing side of the protein.

The measurements of proton transfer in the vicinity of the bound indicator revealed a complex system of interactions between nearby proton-binding sites. Within less than 20 Å from the dye, we observed three functional groups, each with its own kinetic and thermodynamic constants, that interacted through proton transfer with each other and the dye. The conclusions of the kinetic analysis are highly consistent with the structure of the most stable conformation of the dye with respect to the protein surface. Thus, the kinetic measurements provide a basis for determining local conformations of a protein, which are not necessarily those favored during crystallization, yet may be relevant to the function of the enzyme.

REFERENCES

1. Wikström, M. K. F. (1977) *Nature 266*, 271−273.
2. Gennis, R. B. (1998) *Biochim. Biophys. Acta 1365*, 241−248.
3. Gennis, R. B. (1998) *Proc. Natl. Acad. Sci. U.S.A. 95*, 12747−12749.
4. Michel, H. (1998) *Proc. Natl. Acad. Sci. U.S.A. 95*, 12819−12824.
5. Michel, H. (1999) *Biochemistry 38*, 15129−15140.
6. Michel, H. (1999) *Nature 402*, 602−603.
7. Verkhovsky, M. I., Jasaitis, A., Verkhovskaya, M. L., Morgan, J. E., and Wikström, M. (1999) *Nature 400*, 480−483.
8. Wikström, M. (2000) *Biochemistry 39*, 3515−3519.
9. Iwata, S., Ostermeier, C., Ludwig, B., and Michel, H. (1995) *Nature 376*, 660−669.
10. Ostermeier, C., Harrenga, A., Ermler, U., and Michel, H. (1997) *Proc. Natl. Acad. Sci. U.S.A. 94*, 10547−10553.
11. Tsukihara, T., Aoyama, H., Yamashita, E., Tomizaki, T., Yamaguchi, H., Shinzawa-Itoh, K., Nakashima, R., Yaono, R., and Yoshikawa, S. (1995) *Science 269*, 1069−1074.
12. Tsukihara, T., Aoyama, H., Yamashita, E., Tomizaki, T., Yamaguchi, H., Shinzawa-Itoh, K., Nakashima, R., Yaono, R., and Yoshikawa, S. (1996) *Science 272*, 1136−1144.
13. Konstantinov, A. A., Siletsky, S., Mitchell, D., Kaulen, A., and Gennis, R. B. (1997) *Proc. Natl. Acad. Sci. U.S.A. 94*, 9085−9090.
14. Watmough, N. J., Katsonouri, A., Little, R. H., Osborne, J. P., Furlong-Nickels, E., Gennis, R. B., Brittain, T., and Greenwood, C. (1997) *Biochemistry 36*, 13736−13742.
15. Pfitzner, U., Odenwald, A., Ostermann, T., Weingard, L., Ludwig, B., and Richter, O. M. (1998) *J. Bioenerg. Biomembr. 30*, 89−97.
16. Vygodina, T. V., Pecoraro, C., Mitchell, D., Gennis, R., and Konstantinov, A. A. (1998) *Biochemistry 37*, 3053−3061.
17. Karpefors, M., Ädelroth, P., Zhen, Y., Ferguson-Miller, S., and Brzezinski, P. (1998) *Proc. Natl. Acad. Sci. U.S.A. 95*, 13606−13611.
18. Ädelroth, P., Gennis, R. B., and Brzezinski, P. (1998) *Biochemistry 37*, 2470−2476.
19. Brzezinski, P., and Ädelroth, P. (1998) *J. Bioenerg. Biomembr. 30*, 99−107.
20. Karpefors, M., Ädelroth, P., Aagaard, A., Sigurdson, H., Svensson-Ek, M., and Brzezinski, P. (1998) *Biochim. Biophys. Acta 1365*, 159−169.
21. Zaslavsky, D., and Gennis, R. B. (1998) *Biochemistry 37*, 3062−3067.
22. Sinjorgo, K. M., Steinebach, O. M., Dekker, H. L., and Muijsers, A. O. (1986) *Biochim. Biophys. Acta 850*, 108−115.
23. Marantz, Y., Nachliel, E., Aagaard, A., Brzezinski, P., and Gutman, M. (1998) *Proc. Natl. Acad. Sci. U.S.A. 95*, 8590−8595.
24. Yoshikawa, S., Choc, M. G., O'Toole, M. C., and Caughey, W. S. (1977) *J. Biol. Chem. 252*, 5498−5508.
25. Solntsev, M. K., Huppert, D., Tolbert, L., and Agmon, N. (1998) *J. Am. Chem. Soc. U.S.A. 120*, 7981−7982.
26. Einarsdóttir, Ó., Choc, M. G., Weldon, S., and Caughey, W. S. (1988) *J. Biol. Chem. 263*, 13641−13654.
27. Gutman, M. (1984) *Methods Biochem. Anal. 30*, 1−103.
28. Gutman, M., Nachliel, E., and Gershon, E. (1985) *Biochemistry 24*, 2937−2941.
29. Gutman, M. (1986) *Methods Enzymol. 127*, 522−538.
30. Nachliel, E., Yaniv-Checover, S., and Gutman, M. (1997) *Solid State Ionics 97*, 75−92.
31. Shimoni, E., Nachliel, E., and Gutman, M. (1993) *Biophys. J. 64*, 480−483.
32. Gutman, M., and Nachliel, E. (1997) *Annu. Rev. Phys. Chem. 48*, 329−356.
33. Sacks, V., Marantz, Y., Aagaard, A., Checover, S., Nachliel, E., and Gutman, M. (1998) *Biochim. Biophys. Acta 1365*, 232−240.
34. Nachliel, E., Pollak, N., Huppert, D., and Gutman, M. (2001) *Biophys. J. 80*, 1498−1506.
35. Tomizaki, T., Yamashita, E., Yamaguchi, H., Aoyama, H., Tsukihara, T., Shinzawa-Itoh, K., Nakashima, R., Yaono, R., and Yoshikawa, S. (1999) *Acta Crystallogr., Sect. D: Biol. Crystallogr. 55*, 31−45.
36. Sitkoff, D., Ben-tal, N., and Honig, B. (1996) *J. Phys. Chem. 100*, 2744−2752.
37. Gutman, M., and Nachliel, E. (1990) *Biochim. Biophys. Acta 1015*, 391−414.

38. Checover, S., Marantz, Y., Nachliel, E., Gutman, M., Pfeiffer, M., Tittor, J., Oesterhelt, D., and Dencher, N. A. (2001) *Biochemistry 40*, 4281−4292.
39. Lancaster, C. R., Michel, H., Honig, B., and Gunner, M. R. (1996) *Biophys. J. 70*, 2469−2492.
40. Alexov, E. G., and Gunner, M. R. (1999) *Biochemistry 38*, 8253−8270.
41. Malatesta, F., and Capaldi, R. (1982) *Biochem. Biophys. Res. Commun. 109*, 1180−1805.
42. Muller, M., and Azzi, A. (1985) *FEBS Lett. 184*, 110−114.
43. Zhen, Y., Hoganson, C. W., Babcock, G. T., and Ferguson-Miller, S. (1999) *J. Biol. Chem. 274*, 38032−38041.
44. Gutman, M., and Natchliel, E. (1995) *Biochim. Biophys. Acta 1231*, 123−128.

BI010453W